Master's Thesis
석사 학위논문

Study on Growth Mechanism of Atomically Thin WS_2 Crystals and their Characterization

Sunghwan Jo (조 성 환, 趙 星 煥)

Department of Emerging Materials Science

신물질과학전공

DGIST

2015

Master's Thesis
석사 학위논문

Study on Growth Mechanism of Atomically Thin WS_2 Crystals and their Characterization

Sunghwan Jo (조 성 환, 趙 星 煥)

Department of Emerging Materials Science

신물질과학전공

DGIST

2015

Study on Growth Mechanism of Atomically Thin WS_2 Crystals and their Characterization

Advisor : Professor Chang-Hee Cho

Co-advisor : Professor Il-Kyu Park

by

Sunghwan Jo
Department of Emerging Materials Science
DGIST

A thesis submitted to the faculty of DGIST in partial fulfillment of the requirements for the degree of Master of Science in the Department of Emerging Material Science. The study was conducted in accordance with Code of Research Ethics[1]

07. 08. 2015

Approved by

Professor Chang-Hee Cho (Signature)
(Advisor)

Professor Il-Kyu Park (Signature)
(Co-Advisor)

[1] Declaration of Ethical Conduct in Research: I, as a graduate student of DGIST, hereby declare that I have not committed any acts that may damage the credibility of my research. These include, but are not limited to: falsification, thesis written by someone else, distortion of research findings or plagiarism. I affirm that my thesis contains honest conclusions based on my own careful research under the guidance of my thesis advisor.

Study on Growth Mechanism of Atomically Thin WS_2 Crystals and their Characterization

Sunghwan Jo

Accepted in partial fulfillment of the requirements for the degree of Master of Science.

07. 08. 2015

Head of Committee 조 창 희 (인)
Prof. Chang-Hee Cho

Committee Member 박 일 규 (인)
Prof. Il-Kyu Park

Committee Member 서 정 필 (인)
Prof. Jungpil Seo

MS/EM
201321017

조 성 환. Sunghwan Jo. Study on Growth Mechanism of Atomically Thin WS_2 Crystals and their Characterization. Department of Emerging Materials Science. 2015. 39p. Advisor Prof. Cho, Chang-Hee, Co-Advisor Prof. Park, Il-Kyu.

Abstract

Recently, two dimensional atomic-layered transition metal dichalcogenides (TMDCs) such as molybdenum disulfide (MoS_2) and tungsten disulfide (WS_2) have been intensively studied in the last decades due to their semiconducting electronic band structure unlike a metallic graphene. The single-layered TMDCs are very attractive materials for photonic and optoelectronic applications because it has outstanding optical properties including the high quantum yield and the large exciton binding energy reaching up to 1 eV, which are absent in the bulk TMDCs. However, the understanding of nucleation and growth mechanism to realize the large-scale singe-layered TMDCs is still lacking. In this paper, we have studied the two series of single-layered WS_2 crystals which varies the growth temperature and time by using thermal chemical vapor deposition (CVD) method. The powder of sulfur (S) and WO_3 was used as the source and PTAS (Perylen-3, 4, 9, 10-tetracaboxylic acid tetrapotassium salt) was introduced as the promoter for the CVD growth. The as-grown WS_2 crystals show the single layer domain size of ~ 20 μm and the good optical/structural properties. Using the transmission electron microscopy (TEM), atomic force microscopy (AFM), and Raman scattering analyses, we confirmed the nucleation site is formed by the thick single-crystal WS_2 which is not an intermediate form. We demonstrate that growth mode is gradually changed from 3D to 2D as the growth temperature increase 650 ~ 750 °C to 800 ~ 850 °C, indicating the 3D nucleation site is early formed at initial stage and sufficient heat energy is required to facilitate the well-expandable the 2D mode after nucleation. Meanwhile, the ratio of domain- to core-size decreases and the optical property degrades as the growth time increases. These results clearly show that bulk phase of WS_2 has thermodynamical stability compared to 2D phase and source deficient condition is reached with increasing the growth time. Our results offer new insight into the formation of 3D nucleation site in initial growth step and the presence of limited length-scale for the domain size in the growth of single-layered TMDCs.

Keywords: Tungsten disulfide, Two dimensional materials, Growth mechanism, Chemical vapor deposition

Contents

List of tables

List of figures

I. Introduction

1.1 Motivation

Two dimensional (2D) transition metal dichalcogenides (TMDCs) are one of the most famous nanomaterial which is known as graphene-like layered structure since graphene has been found [1]. As the single layer TMDCs such as molybdenum disulfide (MoS_2) and tungsten disulfide (WS2) have been mechanically exfoliated from the bulk crystal, the single layer TMDCs have attracted a great deal of attention as an efficient light emitter due to their semiconducting band structure (bandgap of 1~2eV) [2, 3] unlike metallic graphene. Furthermore, especially among TMDCs, single layer WS_2 has strong photoluminescence (PL) of 20 ~ 40 times higher than that of MoS_2 [4] and large exciton binding energy of 300 ~ 700 meV compared to room temperature of 25 meV [5, 6]. These remarkable optical properties of single layer WS_2 made it possible to design optoelectronic devices such as light emitter diode and laser diode. Recently, single layer TMDCs are expected to tune and manifest their electronic and optical properties by controlling the stacking sequence as inserting other vdW crystals (so-called vdW heterostructure) such as graphene, boron nitride and so on [7-10]. Thus, single layer TMDCs are one of the potential 2D nanomaterial from the view point of scientific to industrial fields in the near future.

Even though new optoelectronic devices based on single layer WS_2 or MoS_2

have been suggested and reported [11-13], the understanding of nucleation and growth mechanism to realize the large-scale singe layered TMDCs is still lacking. As a bottom-up process, chemical vapor deposition (CVD) is one of the most popular methods for the single layer synthesis of WS_2. CVD method provides several benefits including large-scale and uniform synthesis rather than top-down method such as mechanical exfoliation. The studies on nucleation and growth mechanism of large scale TMDCs monolayer during CVD process have been rarely conducted [14-17]. However, because the size of the single layer TMDCs prepared by CVD process is still up to hundreds of micrometers, large scale synthesis is very challenging work.

In this study, we have prepared the two series of single-layered WS_2 crystals by using thermal chemical vapor deposition (CVD) method. We investigate nucleation and growth mechanism of single layered WS_2 dependent on the growth temperature and time, and then systematically trace surface morphology, element composition, and optical properties. Our results clearly show the formation of 3D nucleation site in initial growth step and the presence of limited length-scale for the domain size in the synthesis of single layer WS_2 [4].

1.2 Preceding researches

1.2.1 Growth methods

There are two ways to obtain atomically thin film of the TMDCs: 1) Mechanical peeling from their parent material. 2) Vacuum deposition on the substrate. Because mechanical exfoliation method cannot make the film of uniform and large scale, this method

is not suitable to make electronic devices. On the other hand, vacuum deposition can synthesize large scale of the atomic uniform sheet rather than the mechanical exfoliation method.

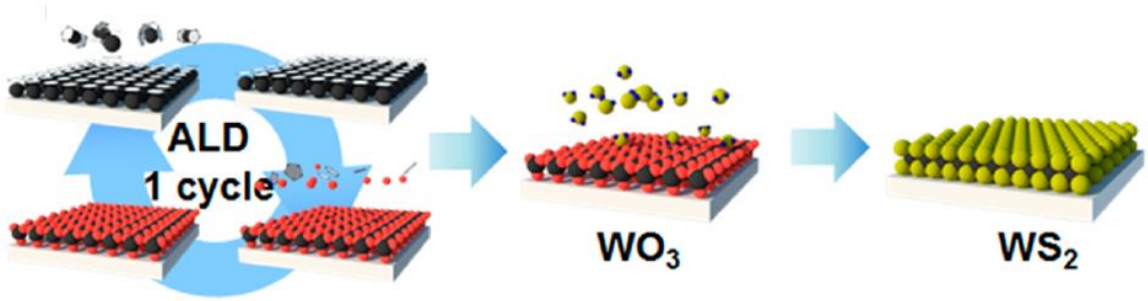

Figure 1. Schemetic illustrations for the precedure of WS_2 monolayer synthesis using ALD [14].

CVD and atomic layer deposition (ALD) are well known growth method for the vacuum deposition. ALD is a sort of vacuum deposition method using the sequential chemical reaction among the precursors of gas phase. So this method can easily make atomically thin film and control the thickness. Ref.16 shows the growth of the single layer film by ALD [14]. As shown figure 1, the whole process is: 1) WO_3 nanosheets are deposited on a SiO_2/Si substrate (285nm) by ALD using $WH_2(iPrCp)_2$ and oxygen plasma. 2) The WO_3 deposited substrate is sulfurized in a tube furnace under argon and H_2S atmosphere. This method can obtain the large scale of WS_2 monolayers and control WS_2 layers by changing the number of cycles of ALD process for WO_3. However, this monolayer film is polycrystalline WS_2 cluster beside CVD process. And the polycrystalline atomic thin film is

expected to have poor electronic and optical properties than single crystal domain because of many grain boundaries [15]. In contrast, CVD process can obtain single crystal domain monolayers.

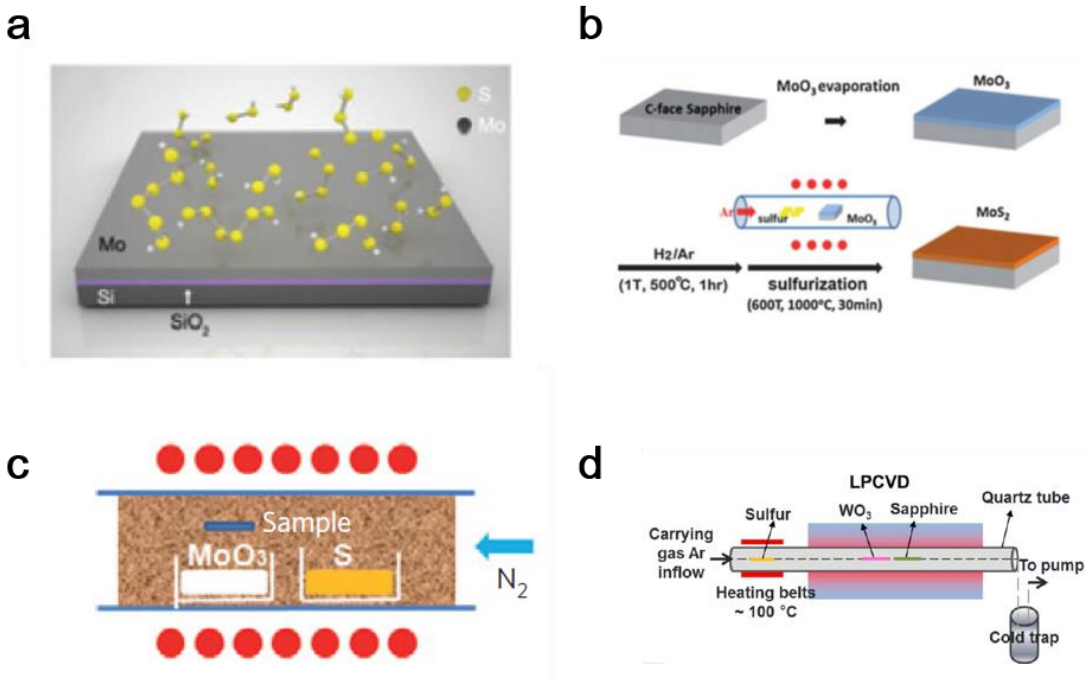

Figure 2. The CVD growth of TMDCs monolayer with (a) transition metal thin film [16], (b) transition metal oxide plate [17], (c) transition metal oxide powder in a one zone furnace [18] and (d) transition metal oxide powder in a one zone furnace and a heating tape for sulfur powder [19].

The CVD process can be roughly separated into one step and two step method. Figure 2 (a) describes the two step CVD method using a thin transition metal film deposited substrate. The prepared substrate was sulfurized in the tube furnace under nitrogen atmosphere after transition metal film (1~2nm) was deposited on a SiO_2 (285nm) / Si substrate by electron beam evaporator. The method had some problems with the thin films. The uniform monolayers could not be obtained through this method because of challenging

thin transition metal deposition uniformly. And the monolayer had metallic electronic properties due to the transition metal impurity [16]. Similarly, figure 2 (b) shows the growth method using sulfurization with CVD after a substrate deposited transition metal oxide microplates. This method reported highly crystalline MoS_2 monolayer could be obtained with controlled layer thickness using various thickness of the transition metal oxide nanocrystals [17, 20] and the continuous single layer film with appropriate patterning of the transition metal oxide flakes which was acted as nucleation sites [21]. However, there is the weak point of two step method that makes the process more complex than one step method because preceding vacuum deposition is needed.

The one step method is the deposition process using chemical reactions of vaporized solid reactants in a tube furnace at the same time. Figure 2 (c) shows one of the most basic one step CVD process that transition metal and sulfur powders are placed into a tube furnace and then are reacted by simultaneously heating in the furnace for depositing on the substrate [18]. This method have been widely used and improved because of its simple procedure. A heating tape was used to restrain rapid vaporization of the sulfur due to its low melting point [19]. One-side sealed quartz tube (opened side was opposite direction of the carrier gas) was placed into a larger quartz tube to maintaining chemical reactions among the reactants [22]. Seed promoters have been used to increase nucleation sites because continuous atomic thin film did not make difficult [23].

1.2.2 Nucleation and growth mechanism

To obtain the large scale of TDMCs, there have been many improvements of the growth method. And some studies have been underway to understand nucleation and growth process for synthesis of large scale of TMDCs monolayer [21, 24, 25]. Figure 3 shows the relationship among pre-deposited MoO_3 thin film, nucleation and growth of MoS_2 during the growth process of MoS_2 monolayer [21]. MoS_2 monolayers grew on randomly deposited MoO_3 nanoribbons and MoO_3 flakes were acted by nucleation site for MoS_2. But the growth didn't progress at the certain point. To overcome the limitation, the dense nucleation sites with artificial step edges were formed to the square patterned MoO_3 (figure 3 (c) and (d)). This edge-based nucleation and growth is similar to theoretical predictions and observations of some other layered materials [26, 27]. Therefore, ref.24 reported similar edge-based catalytic growth also occurs in MoS_2 and are expected to make large scale of continuous TMDCs monolayer.

Seed promoters are used to increase nucleation sites for growth of large size of TMDCs. Figure 4 indicates the changes of MoS_2 growth according to the concentrations of perylene-3,4,9,10-tetracarboxylic acid tetrapotassium salt (PTAS) as a seed promoter [24]. If the concentration of PTAS is too high, size of the monolayers goes small. This result explain the optimal concentration of the seed promoter is needed for the huge size growth. Ref.14 also reported how to act PTAS for the growth process. Effects of PTAS as a seed promoter are: 1) PTAS raise surface energy of the substrate. Thin film growth is effected by surface energy and chemical potential between a substrate and adatoms. If the substrate had larger surface

energy than adatoms, adhesive force between the substrate and adatoms is larger than cohesive force among adatoms. This could be 2D growth easily. 2) PTAS provides heterogeneous nucleation site for WS_2 atoms. Heterogeneous nucleation site helps more facilitating nucleation and growth than homogeneous nucleation site because PTAS makes the surface energy and the free energy barrier of WS_2 lower.

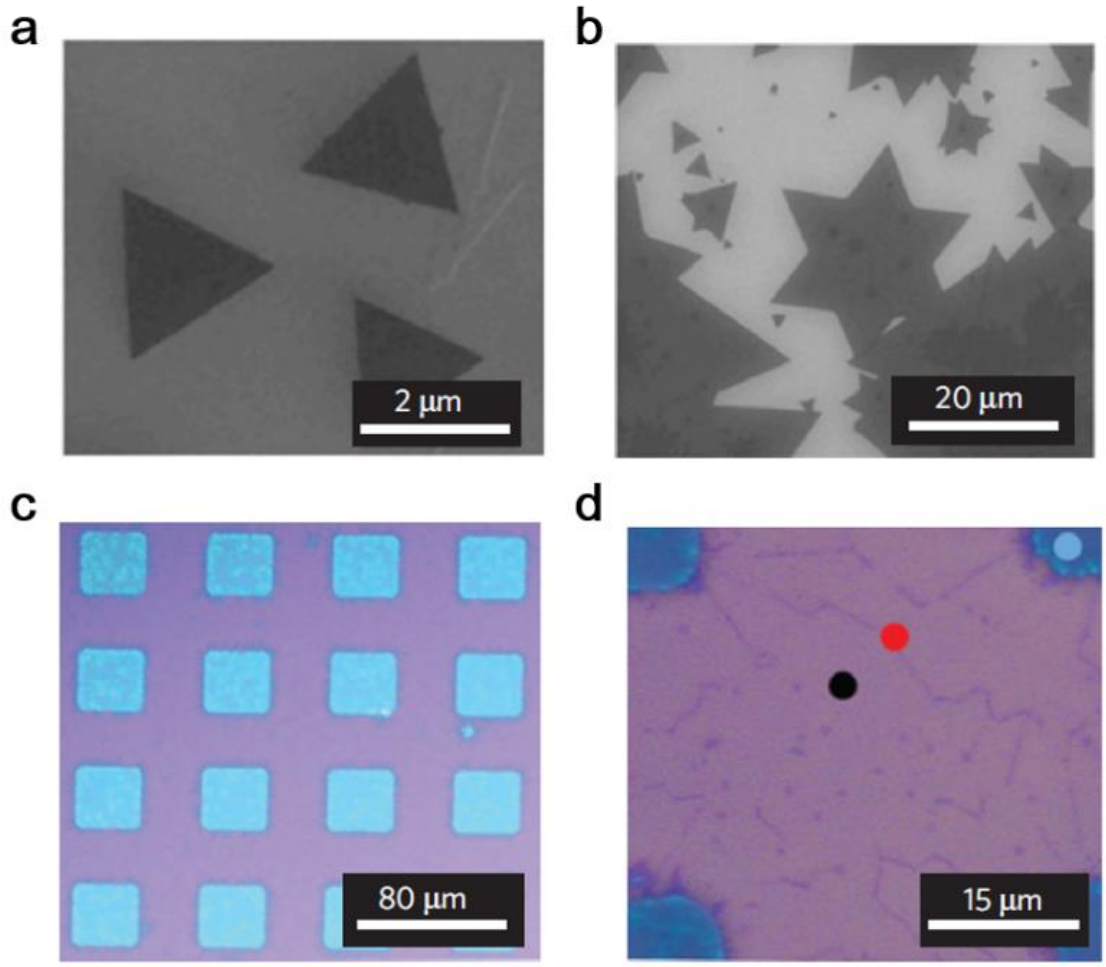

Figure 3. (a) and (b) SEM images of different magnifications. (c) Optical image of continuous MoS_2 film with rectangular patterns of WO_3 on substrates. (d) The magnified optical image of (c) [21].

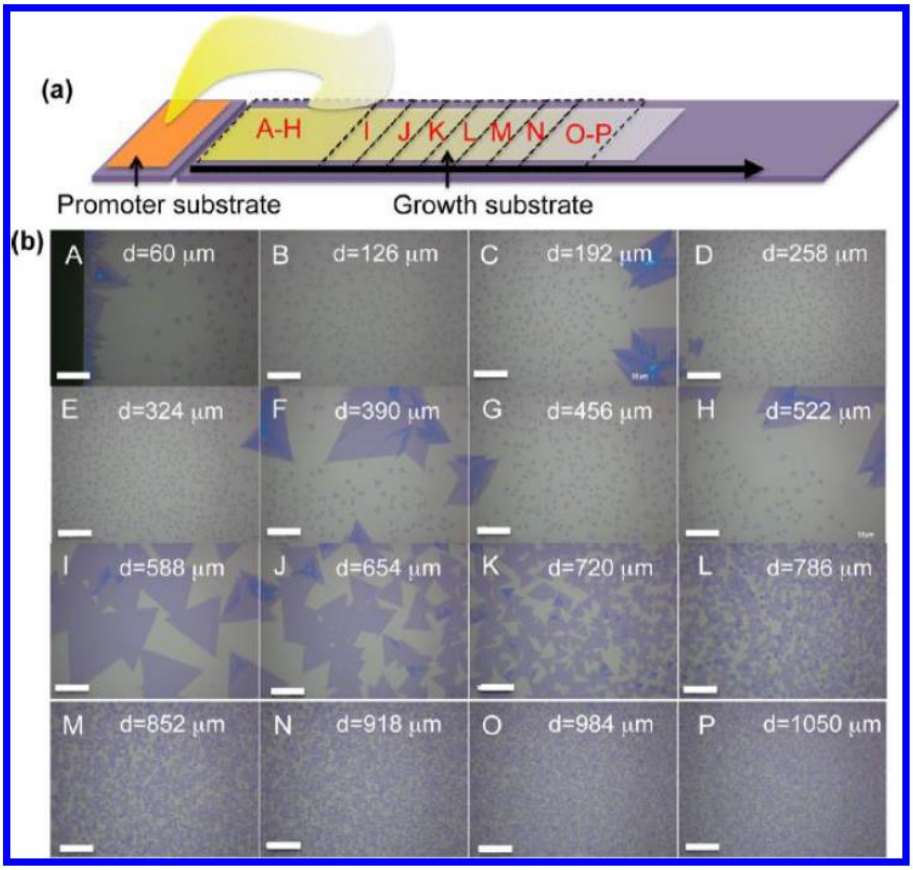

Figure 4. (a) A schemetic diagram of the experimental setup for adjusting the concetrations of the seed promoters as a function of the distance d. (c) Optical images of the MoS_2 monolayers through the distance d [24].

As mentioned previously, if we well understand the nucleation and growth mechanism, we could synthesize the more high quality and large scale of atomically thin film.

1.3 Background principles of nucleation and growth

1.3.1 Homogeneous nucleation

We need to know homogeneous nucleation to understand the deposition and growth process of thin film firstly. Homogeneous nucleation is the basic thermodynamic model to understand heterogeneous nucleation surely. This model is for the system consists of same material. Homogeneous nucleation begins under supersaturation of the vapor. At this time, partial pressure is P_0 and the equilibrium pressure is P_∞. The free energy difference per atom between the vapor and solid is given by [28]

$$G_v = kT \int_{P_0}^{P_\infty} \frac{dP}{P} = -kT \ln\left(\frac{P_0}{P_\infty}\right) = -kT \ln S \quad (1)$$

where $S=P_0 / P_\infty$ is the supersaturation. The difference of free energy per unit volume of solid is [28]

$$\Delta G_v = -nkT \ln S \quad (2)$$

where n is the number of atoms per unit volume of the semiconductor.

Basically embryos under supersaturation (S>1) are in vapor phase. If free energy of the entire system reduced, some embryos grow largely enough. On the other hand, other embryos which smaller than critical embryo size are reevaporating. The critical embryo size is probably determined by volume and surface energy contribution of the embryo. The total free energy for a spherical embryo is derived by [28]

$$\Delta G = \frac{4\pi r^3}{3}\Delta G_v + 4\pi r^2\gamma \quad (3)$$

where γ is the surface free energy per unit area of the solid.

Figure 4.6 indicates the total energy change for two of ΔG_v. Firstly ΔG is increased by the dominant surface energy term, but then if this value approaches a maximum, the free energy difference will be decreased by the free energy reduction because of the predominant phase change. The critical embryo size r_{crit} is affected from the maximum free energy change. If the maximum value is larger which means a larger supersaturation (ΔG_v), the embryo size could be smaller, as shown in figure 5.

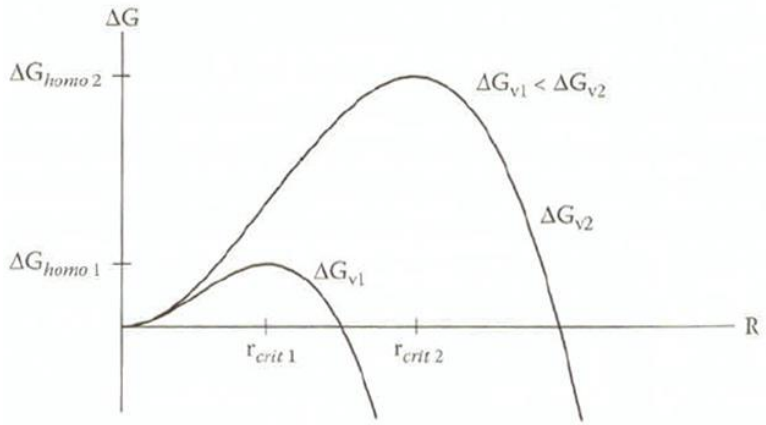

Figure 5. The relationship between the total energy change ΔG and size of the embryo radius R [28].

The critical embryo size can be derived by

$$\left.\frac{\partial \Delta G}{\partial r}\right|_{r=r_{crit}} = 0 \quad (4)$$

which yields

$$r_{crit} = -\frac{2\gamma}{\Delta G_v} \quad (5)$$

Larger embryo size than r_{crit} will have lower free energy which means continuos growth will start. On the other hand, Smaller size of embryo than r_{cirt} will make shrink this embryo because of reducing its free energy. The change in free energy at the critical embryo size can represent as the activation energy for the formation of embryos. This is given by

$$\Delta G_{homo} = \frac{16\pi\gamma^3}{3\Delta G_v^2} \quad (6)$$

1.3.2 Heterogeneous nucleation

To understand the growth process more practically, we have to know heterogeneous nucleation based on the homogeneous model. Heterogeneous nucleation will occur when the chemical composition or crystal structure are different between substrate and thin film. In macroscopic picture, we consider surface free energy among the materials. Assume γ_e and γ_s are the surface free energy of deposited material and substrate, respectively, and γ_i is the interfacial free energy between substrate and the epitaxial layer. The wetting condition of the epitaxial crystal could be different through their surface free energies. If $\gamma_i > (\gamma_e + \gamma_s)$, the epitaxial layer cannot wet the substrate due to the fact that the total surface free energy of this system could increase. On the other hand, complete wetting the substrate is under the surface energy when $(\gamma_e + \gamma_i) < \gamma_s$. Here is the generalized formula of any surface energy combinations where θ is a contact angle between the substrate and an embryo of the epitaxial crystal [29].

$$\gamma_s = \gamma_i + \gamma_e \cos\theta \quad (1)$$

or

$$\theta = \cos^{-1}\left(\frac{\gamma_e - \gamma_i}{\gamma_e}\right) \quad (2)$$

These formulas are well described by figure 6 [28].

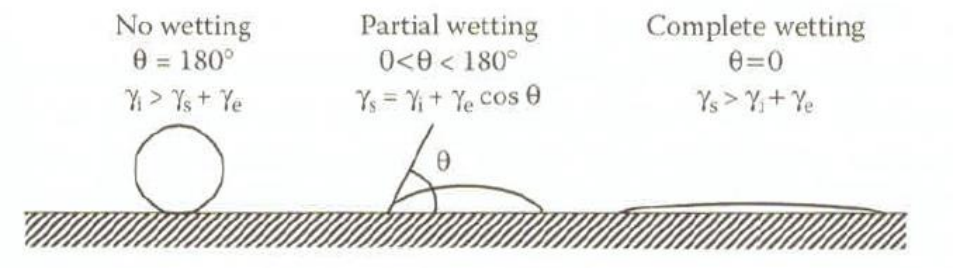

Figure 6. Schematic diagram of wetting of a flat substrate by a droplet. A droplet indicates the epitaxial crystal on the substrate [29].

If we assume the embryos are sphere form with the proper angle θ, we could apply the homogeneous model on the heterogeneous model. The areal change in free energy associated with covering the substrate with the epitaxial layer is indicated by $A_e\gamma_e + A_i(\gamma_i - \gamma_s)$, where A_e and A_i are the embryo surface and interface region. As a result, the total free energy change for a truncated spherical embryo on the substrate is,

$$\Delta G = \frac{\pi r^3}{3}(1-\cos\theta)^2(2+\cos\theta)\Delta G_v + \pi r^2(\gamma_i - \gamma_s)\sin^2\theta + 2\pi r^2(1-\cos\theta)\gamma_e \quad (3)\ [28]$$

where r is the radius of truncated spherical embryo.

Therefore, the activation energy for the formation of embryos is given by

$$\Delta G_{het} = \Delta G_{homo}\left[\frac{(2+\cos\theta)(1-\cos\theta)^2}{4}\right] \quad (4)$$

$$= \frac{16\pi\gamma_e^3(2+\cos\theta)(1-\cos\theta)^2}{12\Delta G_v^2} \quad (5)$$

This means the free energy for the heterogeneous nucleation depends on its contact angle. If the embryo is not wetted, ΔG_{het} would equal to ΔG_{homo} because the contact angle should be 180°. On the other hand, when the contact angle is 0° due to well wetness of the embryo, ΔG_{het} would be zero which means the nucleation and growth could be very easy. This result shows importance of wetness in the heterogeneous nucleation and growth [24].

II. EXPERIMENTAL DETAILS

2.1 Experimental equipment

2.1.1 Thermal Chemical Vapor Deposition

The chemical vapor deposition (CVD) is a deposit method that makes thin solid film on the substrate as a result of complex chemical reaction among vapor species. And the thermal chemical vapor deposition system (TCVD) is categorized using its activated manner. TCVD processes only use thermal energy like resistance heating, radio frequency heating or infrared radiation for the activation method.

Some physical and chemical steps during a CVD process can explain how to deposit materials on the substrate. Summarizing briefly, vapor reactant species transport nearby of the substrate. And reactant species diffuse through the boundary layer. The substrate surface absorbs species of intermediate form or reactant species. These species are deposited by surface migration or heterogeneous reaction and then produce by-product species. The surface desorbs by-product species during the surface reactions [28]. Therefore, thermodynamics and molecular kinetics are necessary to understand basic chemical reactions during the CVD process.

TCVD used in this work, consists of 2 parts. First is pressure control part. This part can make vacuum environment and control pressure of the tube reactor using a rotary

pump and a pressure control valve. The rotary pump can pump this system up to 10^{-4} torr. Second part is reactor part. The reactor of this CVD is the horizontal hot-wall tube reactor which contains Proportional–Integral–Derivative temperature controller. The tube furnace make vaporizing precursors and start chemical reactions for deposit thin film on the substrate located in the quartz tube under the laminar flow regime. Figure 7 describes this CVD system.

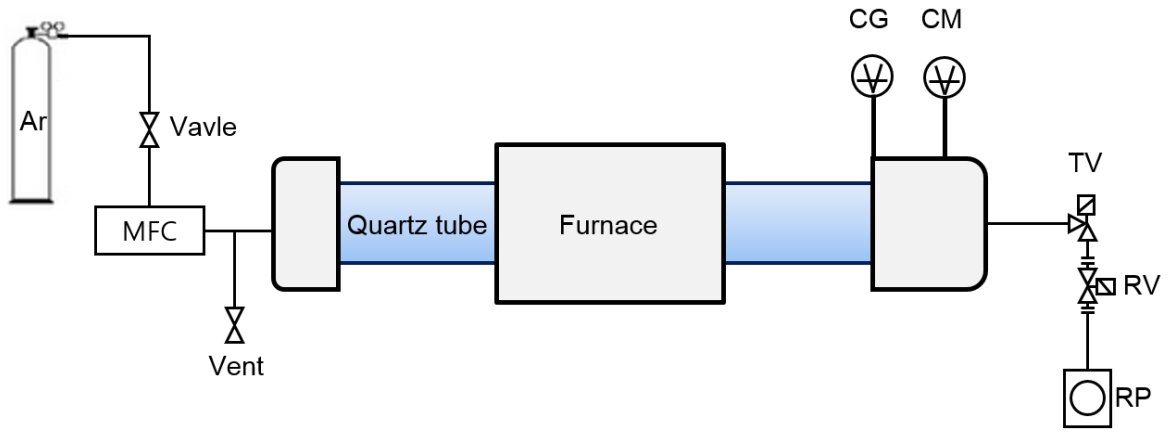

Figure 7. Schematic illustration of the TCVD system.

2.1.2 Photoluminescence

Photoluminescence (PL) spectroscopy is a one of the most common optical characterizing method for semiconducting materials. Luminescence is the radiative emission in solids and therefore, the definition of PL is the luminescence after injecting electron-hole pair by high photon energy.

PL is generally described by interband luminescence in a semiconductor. A semiconductor has electron-hole pairs when electrons in the valence band are excited by

higher photon energy than its bandgap. These electron-hole pairs occur luminescence so that electron-hole pairs recombine each other [30].

Micro PL system used in this work is described on Figure 8. Argon-ion laser at wavelength 457.9nm was used as an excitation light source. The laser intensity before focusing on the sample was reduced by optical density filter. The incident laser was focused on the WS_2 sample through an objective lens of 60 times magnification. Backscattered photons were counted through a monochromator with focal length 30 cm and 300 g/mm grating.

2.1.3 Raman spectroscopy

Raman spectroscopy is an analyzing tool for identifying material's various properties using Raman scattering which is a kind of inelastic scattering from optical phonon. Inelastic scattering, in contrast with elastic scattering, changes the frequencies of scattered light when incident light is scattered by an optical medium.

Micro Raman scattering system used in this work is described on Figure 9. Argon-ion laser at wavelength 457.9nm was used as an excitation light source. No optical density filter was used in this system due to get more Raman scattering signal. The incident laser was focused on the WS_2 sample through an objective lens of 20 times magnification. Backscattered photons were counted through a monochromator with focal length 30 cm and 1200 g/mm grating. And the instrumental spectral resolution was 0.8 cm^{-1}.

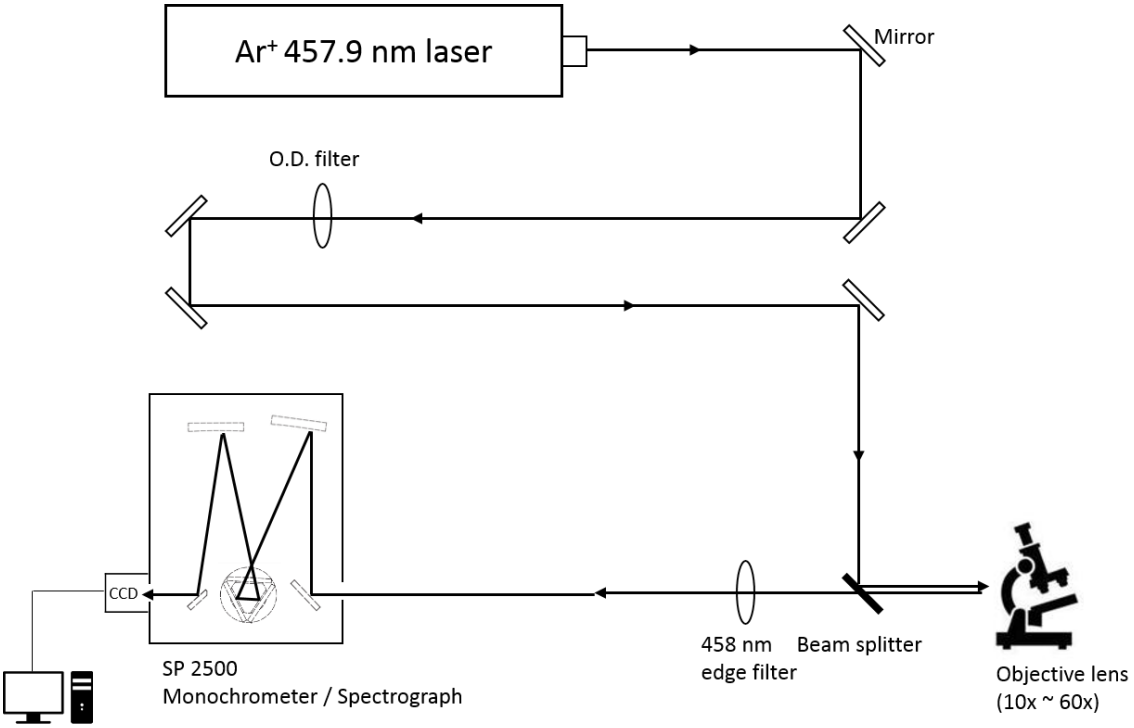

Figure 8. A schematic diagram of home-made micro PL system.

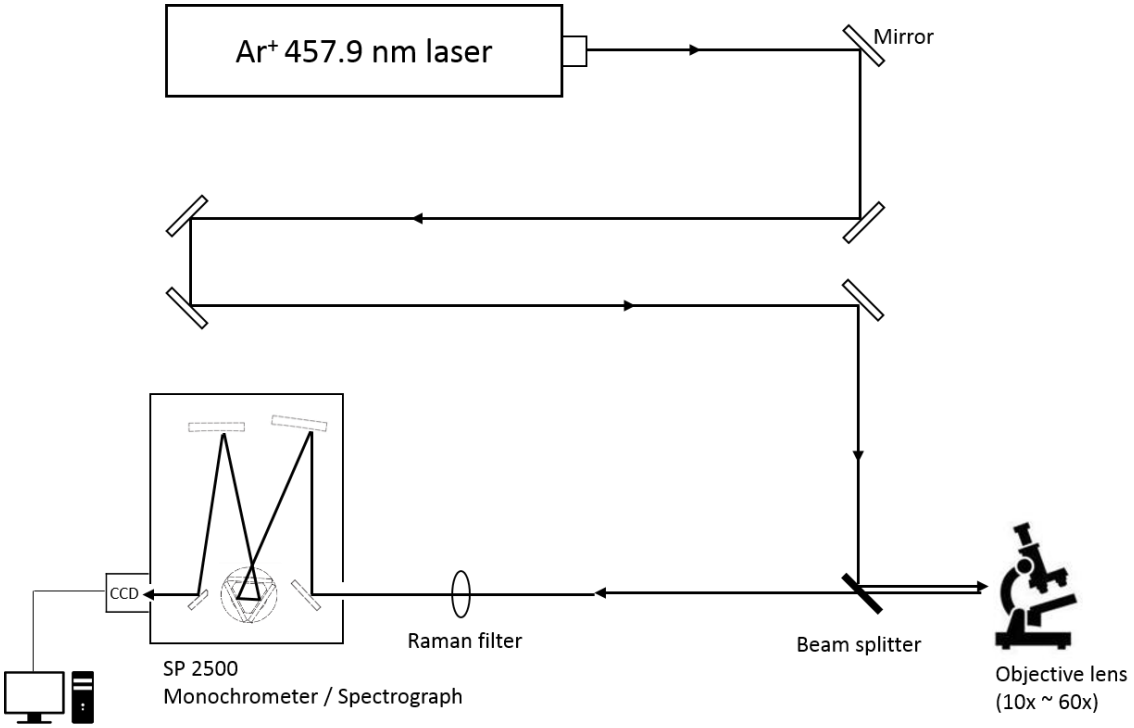

Figure 9. A schematic diagram of home-made micro Raman system.

2.2 Experimental methods

2.2.1 Substrate preparation

The substrates used in this work were one-side polished p-type single crystal Si(100) on SiO_2 layer of 270mn.

The substrate preparation was two step method; substrates cleaning and seed promoter coating. For cleaning, the substrates were sonicated in acetone and methanol to remove some impurities. And then the Si substrates were immersed in hot H_2SO_4, H_2O_2(3:1) mixed solution which called piranha solution to remove residual organic impurities on the substrates and made a hydrophilic surface of the substrates [30]. Producing hydrophilic surface makes the coating process with seed promoter easier. After cleaning process, PTAS was spun on the substrates to help the growth as a seed promoter. Details of these procedures are described in Table I.

Table I. Silicon substrate preparation procedure.

1. Cleaning	**Sonication in acetone for 3 min**
	Sonication in methanol for 3 min
	Rinsing with deionized water 3 times
	Piranha treatment for 2 h
	Rinsing with deionized water 5 times
2. Spin coating	**Spin coating PTAS on substrate with 1000 rpm for 1 min**

2.2.2 WS_2 growth

WS_2 monolayer, in this study, was synthesized by TCVD process. Figure 10 shows experimental setup in TCVD (Figure 2.2.1 a) and specific growth procedure (Figure 10 b). This is a modified method with the conventional growth method of WS_2. The method used different powder precursors, sulfur (S) and tungsten trioxide (WO_3) powder that heated to around 800℃ of high temperatures under inert atmosphere in the tube furnace [18]. Growth substrates were carefully cleaned Si (100) wafer with SiO_2. Cleaning and coating procedures are referring to the above section (2.2.1 Substrate preparation). This substrate and two precursors were loaded into quartz tube (25mm). Si substrate placed face-down above a quartz boat containing 10 mg of WO_3 (99.9%, Sigma Aldrich #101454289). The WO_3 boat located on center of the tube furnace (25mm) and a quartz boat containing 400 mg of S (≥95%, Sigma Aldrich #1001532225) placed upstream from the WO_3 boat.

The CVD process was conducted at 600 torr while flowing ultrahigh-purity argon gas (Ar). Before raising furnace temperature, Ar purging was carried out in 2 hours with 50 s.c.c.m to remove residual gas on the tube surface. After purging, temperature of the furnace raised to 650 ℃ ~ 850 ℃ at 33 ℃ min^{-1} under 600 torr with Ar flow (50 s.c.c.m). And then the temperature held 0 ~ 180 min according to each growth condition. Specific growth conditions are indicated in Table II below. If all reaction was over, the substrate was cooled rapidly as the furnace opened and moved away from the precursors and substrate with high Ar flow (200 s.c.c.m) to stop further chemical reactions.

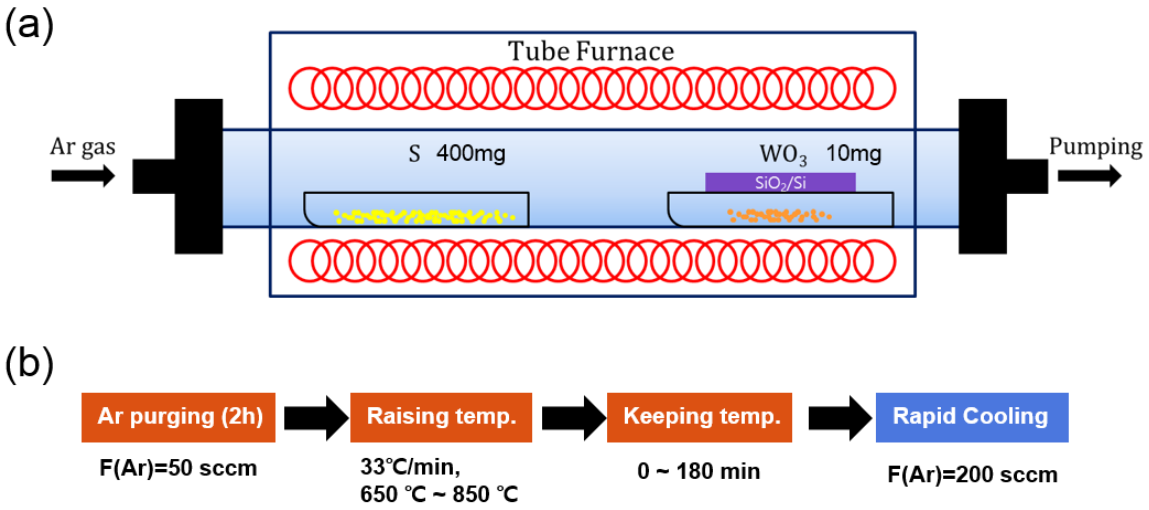

Figure 10. (a) The schematic WS_2 synthesis method using TCVD system. (b) Flow chart for synthesis process of the WS_2 with TCVD.

Table II. Experimental conditions for growth temperature (a) and time(b).

(a)

Time	0 min					
Temperature	650 ℃	700 ℃	750 ℃	800 ℃	850 ℃	

(b)

Time	0 min	10 min	20 min	30 min	50 min	90 min	120 min	150 min	180 min
Temperature	850 ℃								

III. RESULTS AND DISCUSSION

3.1 Surface morphology

We implemented ex-situ experiments through optical images with various growth conditions. This experiment was designed as temperature and reaction time dependent conditions. After the heating process, rapid cooling was conducted to stop further chemical reactions by heat. More details refer to section 2.2.2 and Table II of this paper.

Figure 11 (a) are optical images which describe the reaction temperature dependent conditions of the WS_2 growth. According to these images, WS_2 bulks are observed from 650 ℃ to 750 ℃ and then the thin films are discovered from 800 ℃. These results mean that WS_2 dominantly grow to three-dimension flake by heterogeneous growth with PTAS before the growth temperature reaches to 800 ℃ ~ 850 ℃. And 2D growth will start around 3D clusters synthesized beforehand and the largest amount of single layers are observed when the temperature reaches to 850 ℃. From this data, we can know the growth mode was changed by increasing the growth temperature. Figure 11 (b) shows the relationship between monolayer growth and reaction time at 850 ℃. According to figure 11 (b), All domains have a thick spot at the center of each domain and monolayers grow along a thick WS_2 flake until 20 min and then shrink by specific size. This means thick spots of WS_2 act as a nucleation site. The size of monolayers change the thick islands (core) at the center of each triangular sheet, which is nucleation site in the initial growth stage, grow

gradually after 20 min. And thereafter, monolayers are completely evaporated at 180 min. Size change of monolayers and cores can confirm more clearly with figure 12. Figure 12 shows size of the crystal domain and core regarding various temperatures. In figure 12 (a), the size of crystal domain increases until 20min and then saturates to specific size. Size of monolayers drastically decrease in 120 min where saturated size of the domains decreases. And finally all monolayers were disappeared at 150 min ~ 180 min. Through these data, we can know the growth condition of 850 ℃, 20 min is the best condition for monolayer synthesis.

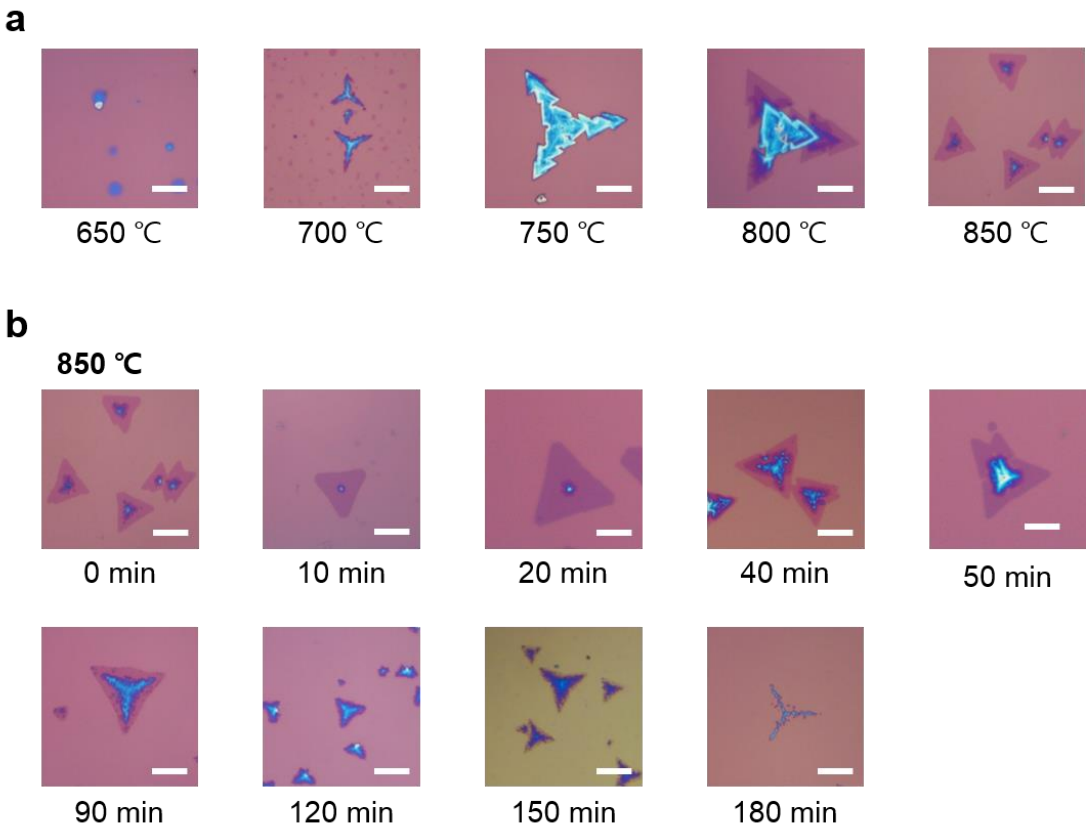

Figure 11. Optical microscopy images of CVD-grown WS_2 crystals with varying the experimental conditions for temperature (a) and time (b). All scale bars indicate 10 ㎛.

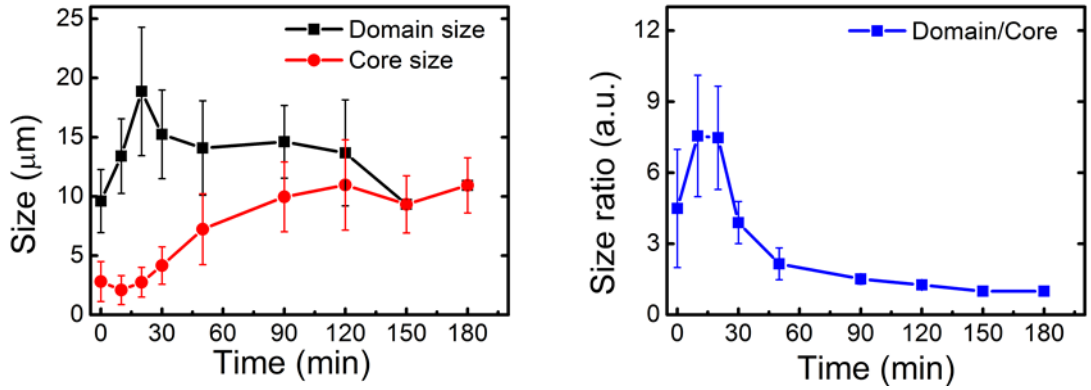

Figure 12. (a) Crystal domain (black) and nucleus (red) size of WS_2 as a function of growth time. (b) This figure indicates ratio of the domain size to the nucleus size. The ratio decreases after 20 minutes of the growth time. (a) and (b) are the statistically analyzed data taken from 100 WS_2 crystals per each growth conditions. Each point is the average value for the conditions and the error bar indicates the standard deviation.

3.2 Nucleation site

After synthesis process, we investigated some properties of WS_2 triangular sheet of a nucleation site to understand for nucleation and growth of WS_2 monolayer analyzing the best sample for monolayer growth (850 ℃, 20 min). Firstly, Raman scattering carried out to identify whether this material was WS_2 or not and predict its thickness through checking the space between two Raman-active mode of WS_2. And we confirmed the thickness of this WS_2 flake using atomic force microscopy (AFM). Finally we implemented transmission electron microscopy (TEM) and energy-dispersive X-ray spectroscopy (EDS) to investigate crystal structure and chemical composition of the nucleation site and WS_2 sheet.

Figure 13 (a) is an image of WS_2 triangular sheet and Raman scattering conducted at the core and side. WS_2, same as MoS_2, belongs to the space group D_{6h} ($P6_3/mmc$) which has two Raman-active modes of E^1_{2g} and A_{1g} [31]. Figure 13 (b) shows the Raman spectra at the core and side that could confirm E^1_{2g} and A_{1g} mode of WS_2. The peak position of the E^1_{2g} mode at the core is 356.8 cm^{-1} and the same mode at the side is 357.4 cm^{-1}. A_{1g} modes at the core and side are respectively 420.6 cm^{-1} and 418.3 cm^{-1}. The peak differences between the E^1_{2g} and A_{1g} mode at the core ($\Delta\omega_{core}$) and side ($\Delta\omega_{side}$) are respectively 63.8 cm^{-1} and 60.9 cm^{-1} due to their thickness. The frequencies of E^1_{2g} and A_{1g} mode in WS_2 depend on the thickness because vdW interlayer interaction changes effective restoring force of each vibration mode if the number of layer of the WS_2 changed. And the more WS_2 is thick, the more the frequency difference increase because of increased stiffness of the two Raman-active modes [32]. Therefore, the B is thicker than the S and we can infer that the S is single layer according to data of previous works [33, 34].

To confirm the thickness of synthesized WS_2 sheet, we used atomic microscopy to measure the surface geometry. Figure 13 (c) and (d) are topography and height profiles measured by AFM (Park system, XE150) contact mode. According to the topography, WS_2 nanosheet generally contains uniform surface but thick WS_2 of triangular shape was observed at the center region. Thickness of the uniform surface is 0.9nm which is well matched by previously reported values of single-layer WS_2 [22, 34]. The thick triangular flake is 5.8 nm (6~7 layer) and surrounded by double-layered WS_2. Through the Raman and AFM data, we could confirm basic information of the nucleation site such as its

thickness and vibrational mode.

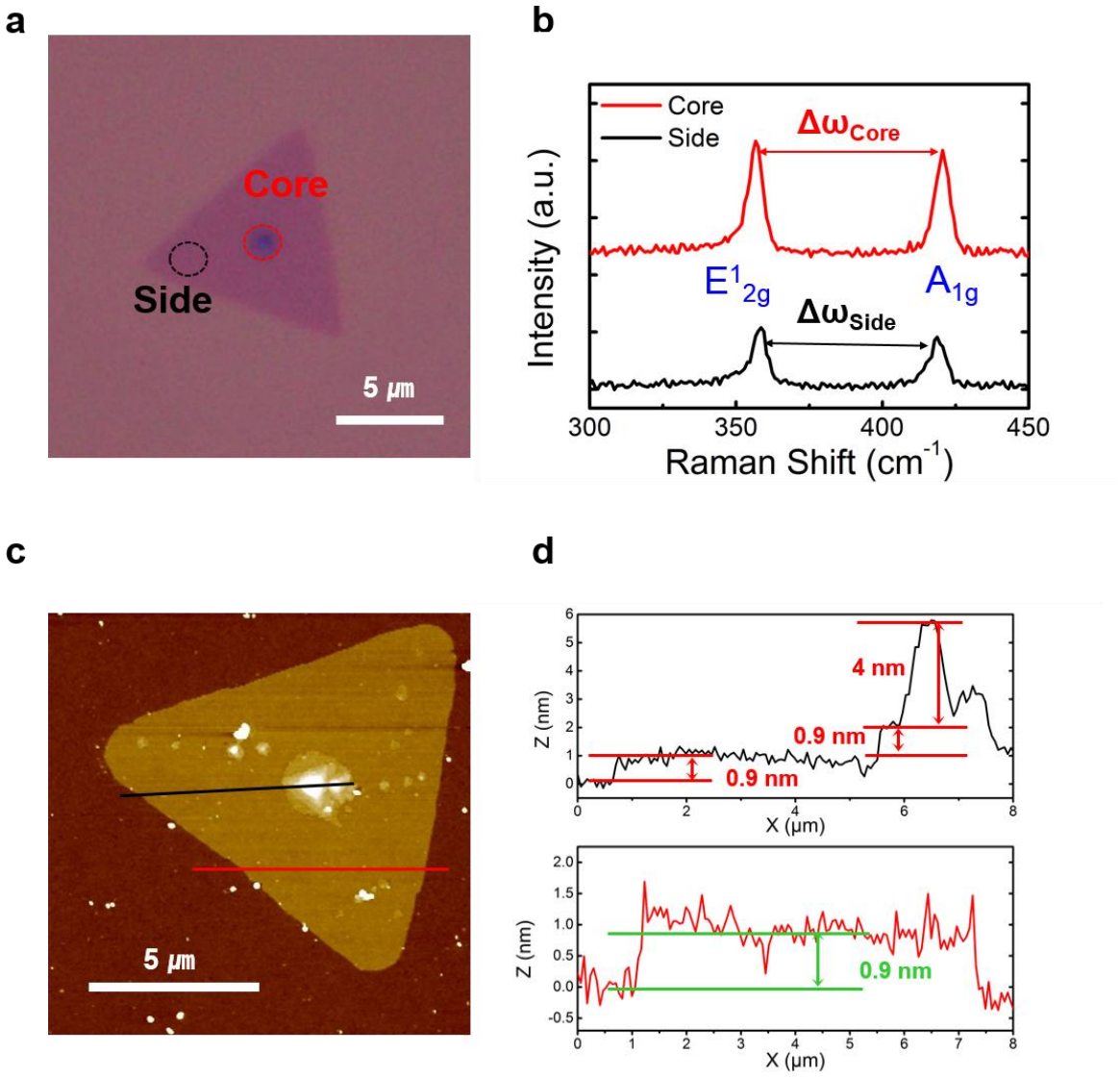

Figure 13. (a) Optical microscopy image of WS_2 triangular sheet. (b) Raman spectra of WS_2 triangular sheet at core and side of (a). The peaks were fitted by single lorentzian functions. (c) AFM image of a WS_2 triangular sheet. A core of triangular shape is observed clearly. (d) AFM height profile with contact mode. Red and green lines indicate the thickness of monolayer and nucleation site of WS_2, respectively

We conducted further experiments of the nucleation site to understand the nucleation and growth. If the core of WS_2 works as a nucleation site in the initial growth stage, identifying its chemical composition could be good information for discovering the growth mechanism. Previous studies reported thick area of WS_2 nanosheet grown by CVD might be an intermediate because sulfur ratio between thick and monolayer part is different and this ratio differences are caused that WO_3 have not a direction reaction of sulfurization [22, 35]. If the nucleation site – the thick part of WS_2 is an intermediate, its crystal structure and ratio of its chemical compositions would be different to the monolayer area. Therefore, we implemented selected area electron diffraction (SAED), high resolution TEM (HR-TEM) to estimate chemical composition of WS_2 core and monolayer through investigating crystal structures of the core and monolayer part and energy dispersive X-ray spectroscopy (EDS) to identify chemical composition and ratio of their chemical species. WS_2 was transferred onto a carbon coated 400 mesh copper grid (TED PELLA, Inc) to load the TEM. In this study, TEM we used was commercial instrument (Hitachi, HF-330). Transfer method referred to ref. 24. Contrary to expectations, we discovered the core and monolayer had a same single crystal structure from the SAED patterns (figure 14 (b) and (c)) and monolayer part has the hexagonal crystal structure (figure 14(d) which space between two tungsten atoms is well matched with theoretic values and X-ray diffraction data [36]. These results are important evidences the core area is not an intermediate. TEM-EDS results enhanced these results. Figure 15 shows EDS mapping result of tungsten and sulfur. Figure 15 (b) and

(c) indicate EDS signals of tungsten and sulfur atoms are entirely observed on this triangular sheet. And ratio of sulfur atoms at the core is almost same as monolayer part.

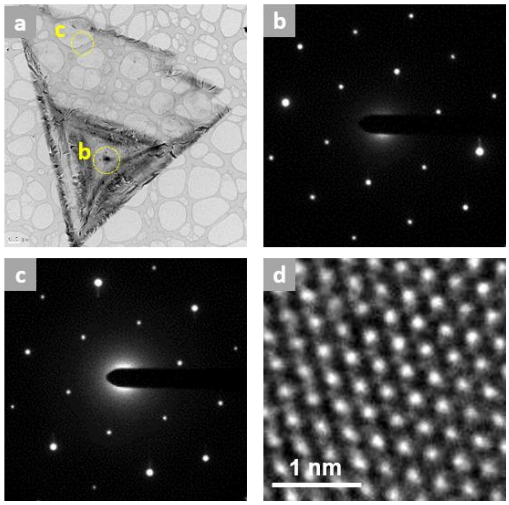

Figure 14. (a) Low magnification bright field TEM image of WS_2 triangular flake. (b) SAED pattern of the nucleation site. The pattern demonstrates multilayered nucleation area consists of single phase of WS_2. (c) SAED pattern from WS_2 side area. This pattern demonstrates it is a single crystal. (d) HR-TEM image acquired from same area as (c). Bright dots are tungsten atoms and lighter dots are sulfur atoms.

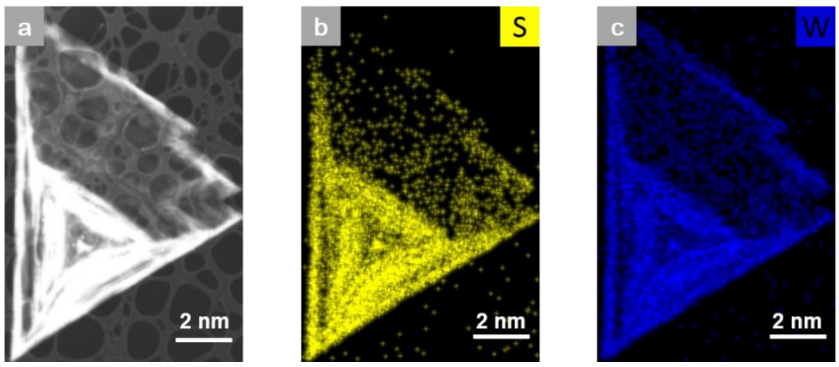

Figure 15. (a) Bright field TEM image with low magnification. (b) and (c) TEM - EDS mapping images. These show sulfur (yellow, (b)) and tungsten (blue, (c)) atoms in the WS_2 triangular flake.

3.3 Growth mechanism

The schematic diagrams, figure 16 (a)-(e), describe the growth process based on the data in this section. The growth process in chronological order is: (a) WS_2 molecules start heterogeneous nucleation on PTAS after WO_3 and S powder decomposed and reacted by heat. PTAS the seed promoter which has graphene-like flat ring structure helps with heterogeneous nucleation of WS_2 flake on the substrate and furthermore, PTAS reduces the nucleation energy of WS_2 because this seed promoter makes the substrate to hydrophilic surface [18, 24]. (b) Thick WS_2 nuclei are created. Previous study reported MoS_2 monolayer is metastable rather than bulk MoS_2 because the formation energy of bulk MoS_2 is lower than MoS_2 monolayer; the formation energy was calculated by fist principle density functional theory [37]. This means the sufficient high reaction temperature is need for the 2D growth. At that time, thick WS_2 flakes are formed to single crystal WS_2 not an intermediate according to section 3.2. (c) The 2D growth starts along the thick single crystal WS_2 nucleus because WS_2 nucleus acts step edge which reduces nucleation barrier and formation energy according to previous studies for graphene growth [27, 38]. During the process between (c) and (d), monolayers don’t grow to the particular size. The critical growth size is believed to be

limited by the diffusion length of WS_2 molecules for 2D growth. Because the 3D growth starts at the next growth step as domain sizes are saturated to specific value. This means the flux of the reactants is not deficient and this size saturation is not caused by concentration changes of the reactants. (d) In this step, WS_2 tend to decrease the size of monolayers and increase the size of nuclei. Because 3D growth at the core is easier than the side area due to the limit of diffusion length according to our assumption and bulk phase is thermodynamically stable than 2D phase. For these reasons, the nucleus size is increasing. Simultaneously, WS_2 sheets undergo thermal thinning effect due to its long exposure time at the high reaction temperature [39]. And the monolayer only evaporate because of the limitation of diffusion length although WS_2 monolayer and nucleus can be evaporated. (e) All monolayers are evaporated and bulks are partially survived. Overexposed samples under the high temperature are almost evaporated even some part of bulk. The reason is flux of the reactants is deficient at this step.

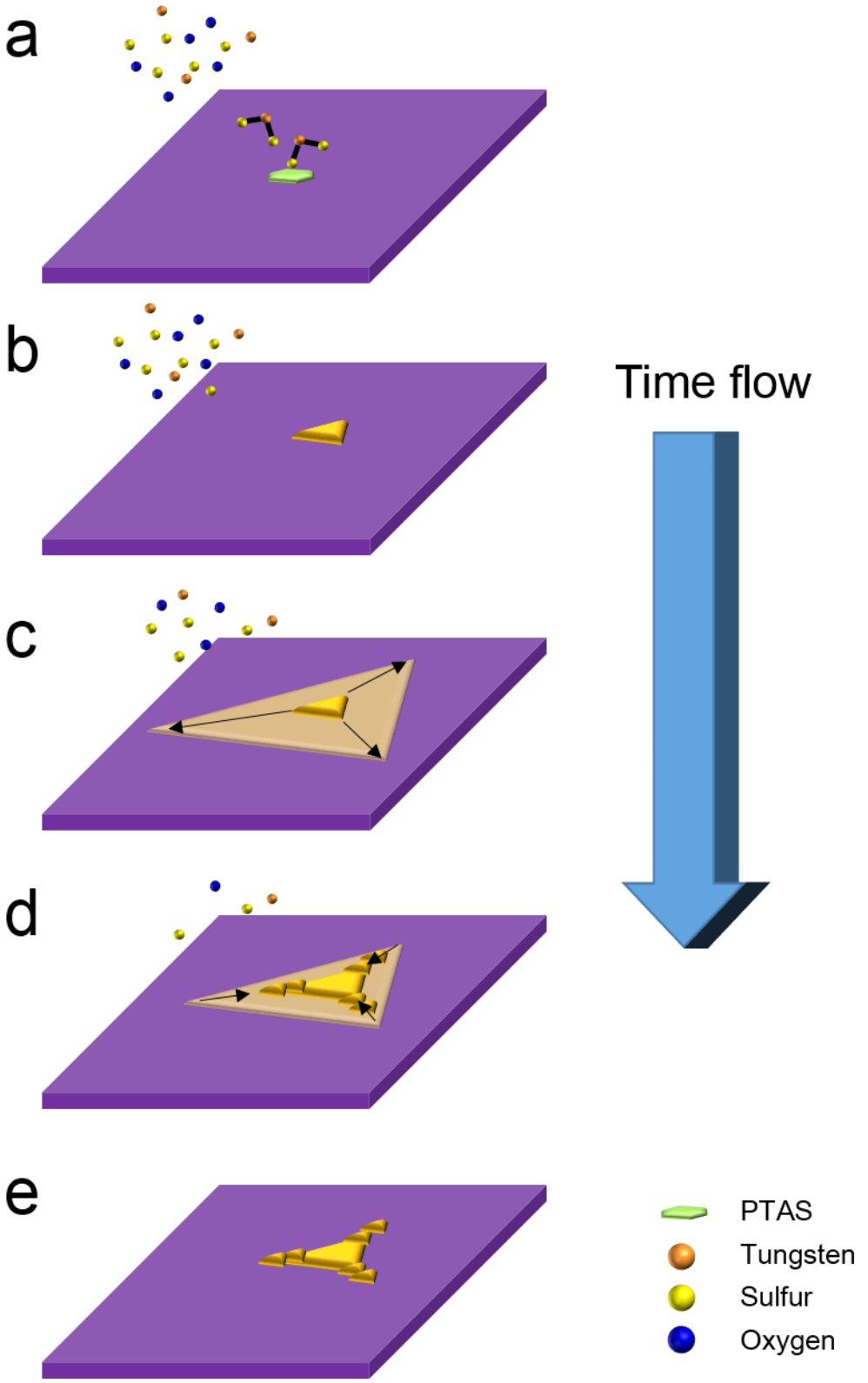

Figure 16. Schematic diagrams for WS_2 growth procedure with time flow. (a)-(d) describe growth process with vaporized reactants. A green flake, orange, yellow, blue balls indicate PTAS, tungsten, sulfur and oxygen atoms respectively.

3.4 Optical characterization

Systematically synthesized WS_2 samples were conducted by optical characterization using Raman and PL spectroscopy to investigate optical properties and find the optimal condition. We used home-made equipment for optical characterization and details refer to section 2.1.2-2.1.3.

We implemented Raman scattering to identify crystallinity and thickness of WS_2 triangular sheet. Figure 17 is the Raman spectra of time dependent conditions. Figure 17 (b) indicates E^1_{2g} (black square), A_{1g} (black triangle) and differences of the two Raman modes corresponding to each conditions. This figure shows Raman-active modes start to change their frequencies after 90 min. After 90 min, frequency difference increase gradually and then the difference nearly approaches bulk value (64.44 cm^{-1}) at 180 min. However, crystal quality between synthesized bulk and monolayer seems not quite a lot of difference because each mode of the spectra has similar full width at half maximum (FWHM).

WS_2 has a tremendous property photoluminescence intensity of A-exciton is remarkably increasing when the crystal become single layer likewise MoS_2 [8]. We measured PL intensity, peak position and FWHM of A-exciton to evaluate optical property of synthesized WS_2 in this work. Figure 18 (a)-(d) indicate PL spectra of the reaction time. We didn't measure PL from 120 min because of their very poor PL intensity. There are no significant changes of A-exciton peak position of WS_2 monolayer until 90 min. So, ununiformed PL emit from 90 min because thick WS_2 are rapidly created on monolayer from this time. PL intensity tends to decrease gradually after 20 min and FWHM tends to increase

after 20 min. Therefore, the temperature holding time shouldn't be over 20 min if you want to obtain WS_2 monolayer of good optical property.

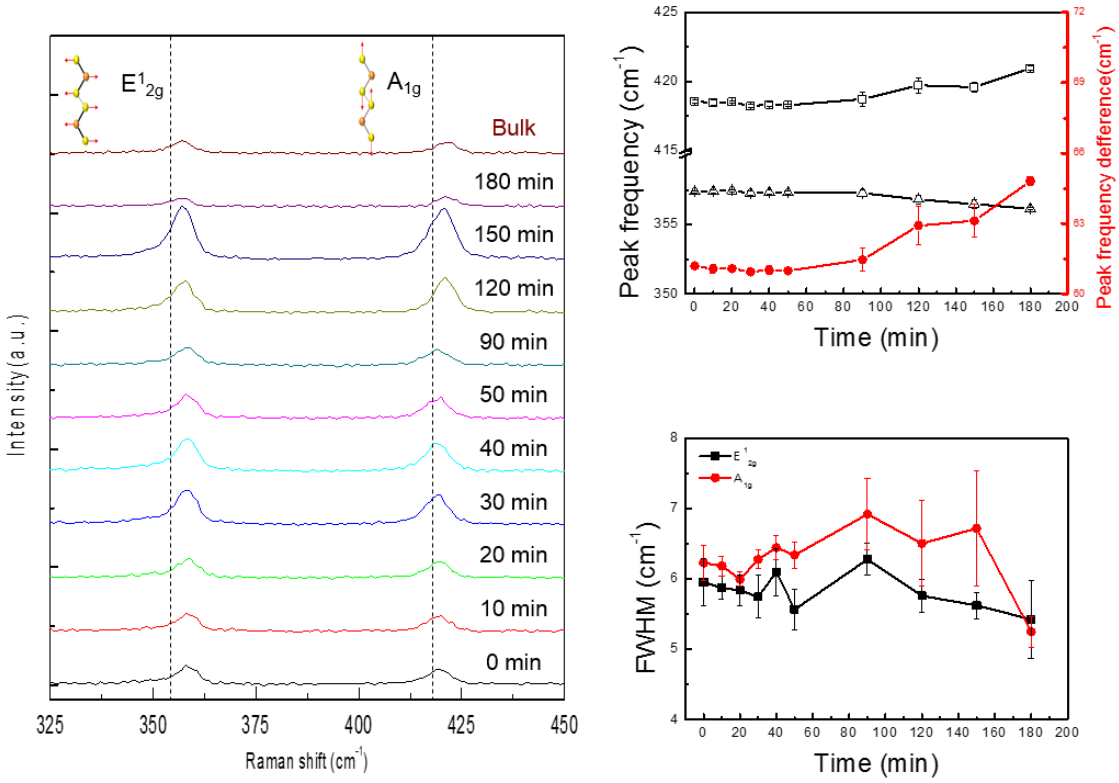

Figure 17. (a) Raman spectra for WS_2 samples of several time conditions with 457.9nm excitation laser. (b) Frequencies for E^1_{2g} (black square), A_{1g} modes (black triangle), their difference in the peak position (red circle), (c) FWHM for E^1_{2g} (black) and A_{1g} modes (red) of all reaction time. The data of (b)(c) were measured 5 times per each growth conditions. Each points are average of the conditions and error bar were calculated by standard deviation.

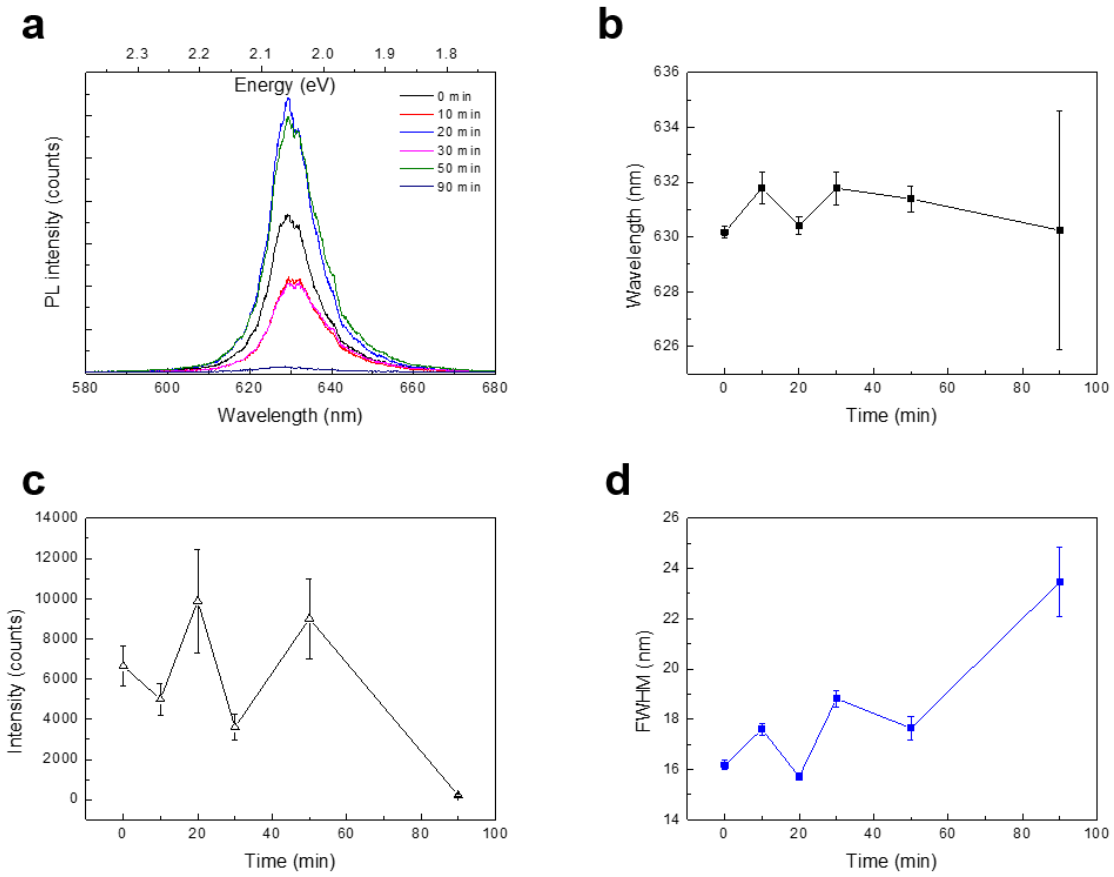

Figure 18. (a) PL spectra of WS_2 samples for growth time with 457.9 nm excitation light. (b) Peak positions, (c) PL intensity and (d) FWHM of A exciton in PL spectra. The data of (b)(c)(d) were measured 5 times per each growth conditions. Each points are average of the conditions and error bar were calculated by standard deviation.

IV. CONCLUSION

We have synthesized two-series of single layer WS_2 crystals using CVD method at various growth temperature and time. The initial nucleation and growth mechanism of single layer WS_2 during the growth have studied by observation of the surface morphology, crystal structure (chemical composition), and optical properties dependent on growth condition. Our results provide the new information about initial nucleation and growth step of thin layer WS_2 prepared by CVD as follows: 1) Formation of single layer which can be driven toward the 2D growth is promoted by sufficient heat energy and the nucleation site of centered triangular crystal (single crystal, not intermediate phase) is formed at initial growth step. 2) The critical 2D size of single layer WS_2 is believed to be limited by the diffusion length attributed to deficient reactant and thermodynamic stability of 3D bulk phase during the growth. 3) The optimal growth condition of large-scale single layer WS_2 was obtained from observation of surface morphology and optical characterizations (Raman scattering and PL spectroscopy). This work offers new insight into the formation of 3D nucleation site at initial growth step and the presence of limited length-scale for the domain size in the growth of single-layered TMDCs. Due to the lack of understanding of growth mechanism compared to large-scale synthesis of TMDCs in the last few years, we believe that our studies offer sufficient consideration in design of optimal growth step for synthesis of large scale single-layered TMDCs.

References

1. Novoselov, K.S., et al., *Two-dimensional atomic crystals.* Proceedings of the National Academy of Sciences of the United States of America, 2005. **102**(30): p. 10451-10453.
2. Mak, K.F., et al., *Atomically Thin MoS_2: A New Direct-Gap Semiconductor.* Physical Review Letters, 2010. **105**(13).
3. Kuc, A., N. Zibouche, and T. Heine, *Influence of quantum confinement on the electronic structure of the transition metal sulfide TS_2.* Physical Review B, 2011. **83**(24).
4. Zhao, W.J., et al., *Evolution of Electronic Structure in Atomically Thin Sheets of WS_2 and WSe_2.* Acs Nano, 2013. **7**(1): p. 791-797.
5. Chernikov, A., et al., *Exciton Binding Energy and Nonhydrogenic Rydberg Series in Monolayer WS2.* Physical Review Letters, 2014. **113**(7).
6. Ye, Z.L., et al., *Probing excitonic dark states in single-layer tungsten disulphide.* Nature, 2014. **513**(7517): p. 214-218.
7. Geim, A.K. and I.V. Grigorieva, *Van der Waals heterostructures.* Nature, 2013. **499**(7459): p. 419-425.
8. Fang, H., et al., *Strong interlayer coupling in van der Waals heterostructures built from single-layer chalcogenides.* Proceedings of the National Academy of Sciences of the United States of America, 2014. **111**(17): p. 6198-6202.
9. van der Zande, A.M., et al., *Tailoring the Electronic Structure in Bilayer Molybdenum Disulfide via Interlayer Twist.* Nano Letters, 2014. **14**(7): p. 3869-3875.
10. Gong, Y.J., et al., *Vertical and in-plane heterostructures from WS_2/MoS_2 monolayers.* Nature Materials, 2014. **13**(12): p. 1135-1142.
11. RadisavljevicB, et al., *Single-layer MoS_2 transistors.* Nat Nano, 2011. **6**(3): p. 147-150.
12. Yoon, Y., K. Ganapathi, and S. Salahuddin, *How Good Can Monolayer MoS_2*

Transistors Be? Nano Letters, 2011. **11**(9): p. 3768-3773.

13. Zhang, Y.J., et al., *Ambipolar MoS_2 Thin Flake Transistors.* Nano Letters, 2012. **12**(3): p. 1136-1140.
14. Song, J.G., et al., *Layer-Controlled, Wafer-Scale, and Conformal Synthesis of Tungsten Disulfide Nanosheets Using Atomic Layer Deposition.* Acs Nano, 2013. **7**(12): p. 11333-11340.
15. van der Zande, A.M., et al., *Grains and grain boundaries in highly crystalline monolayer molybdenum disulphide.* Nature Materials, 2013. **12**(6): p. 554-561.
16. Zhan, Y.J., et al., *Large-Area Vapor-Phase Growth and Characterization of MoS_2 Atomic Layers on a SiO_2 Substrate.* Small, 2012. **8**(7): p. 966-971.
17. Lin, Y.C., et al., *Wafer-scale MoS_2 thin layers prepared by MoO3 sulfurization.* Nanoscale, 2012. **4**(20): p. 6637-6641.
18. Lee, Y.H., et al., *Synthesis of Large-Area MoS_2 Atomic Layers with Chemical Vapor Deposition.* Advanced Materials, 2012. **24**(17): p. 2320-2325.
19. Zhang, Y., et al., *Controlled Growth of High-Quality Monolayer WS_2 Layers on Sapphire and Imaging Its Grain Boundary.* Acs Nano, 2013. **7**(10): p. 8963-8971.
20. Elias, A.L., et al., *Controlled Synthesis and Transfer of Large-Area WS_2 Sheets: From Single Layer to Few Layers.* Acs Nano, 2013. **7**(6): p. 5235-5242.
21. Najmaei, S., et al., *Vapour phase growth and grain boundary structure of molybdenum disulphide atomic layers.* Nature Materials, 2013. **12**(8): p. 754-759.
22. Cong, C.X., et al., *Synthesis and Optical Properties of Large-Area Single-Crystalline 2D Semiconductor WS_2 Monolayer from Chemical Vapor Deposition.* Advanced Optical Materials, 2014. **2**(2): p. 131-136.
23. Lee, Y.H., et al., *Synthesis and Transfer of Single-Layer Transition Metal Disulfides on Diverse Surfaces.* Nano Letters, 2013. **13**(4): p. 1852-1857.
24. Ling, X., et al., *Role of the Seeding Promoter in MoS_2 Growth by Chemical Vapor*

Deposition. Nano Letters, 2014. **14**(2): p. 464-472.

25. Hansen, L.P., et al., *Growth Mechanism for Single- and Multi-Layer MoS_2 Nanocrystals.* Journal of Physical Chemistry C, 2014. **118**(39): p. 22768-22773.
26. Han, G.H., et al., *Influence of Copper Morphology in Forming Nucleation Seeds for Graphene Growth.* Nano Letters, 2011. **11**(10): p. 4144-4148.
27. Gao, J.F., et al., *Graphene Nucleation on Transition Metal Surface: Structure Transformation and Role of the Metal Step Edge.* Journal of the American Chemical Society, 2011. **133**(13): p. 5009-5015.
28. Yongdong, X. and X.-T. Yan, *Chemical vapour deposition : an integrated engineering design for advanced materials*. Engineering materials and processes,. 2010, London ; New York: Springer. xiv, 342 p.
29. Ghandhi, S.K., *VLSI fabrication principles : silicon and gallium arsenide*. 2nd ed. 1994, New York: Wiley. xxiv, 834 p.
30. Grim, R.E., *Applied clay mineralogy*. International series in the earth sciences. 1962, New York,: McGraw-Hill. 422 p.
31. Verble, J.L. and T.J. Wieting, *Lattice Mode Degeneracy in MoS_2 and Other Layer Compounds.* Physical Review Letters, 1970. **25**(6): p. 362-&.
32. Molina-Sanchez, A. and L. Wirtz, *Phonons in single-layer and few-layer MoS_2 and WS_2.* Physical Review B, 2011. **84**(15).
33. Gutierrez, H.R., et al., *Extraordinary Room-Temperature Photoluminescence in Triangular WS_2 Monolayers.* Nano Letters, 2013. **13**(8): p. 3447-3454.
34. Berkdemir, A., et al., *Identification of individual and few layers of WS_2 using Raman Spectroscopy.* Scientific Reports, 2013. **3**.
35. van der Vlies, A.J., et al., *Basic reaction steps in the sulfidation of crystalline tungsten oxides.* Journal of Physical Chemistry B, 2002. **106**(13): p. 3449-3457.
36. Schutte, W.J., J.L. Deboer, and F. Jellinek, *Crystal-Structures of Tungsten Disulfide and*

Diselenide. Journal of Solid State Chemistry, 1987. **70**(2): p. 207-209.

37. Cheng, Y.C., et al., *Van der Waals epitaxial growth of MoS_2 on SiO_2/Si by chemical vapor deposition.* Rsc Advances, 2013. **3**(38): p. 17287-17293.
38. Chen, H., W.G. Zhu, and Z.Y. Zhang, *Contrasting Behavior of Carbon Nucleation in the Initial Stages of Graphene Epitaxial Growth on Stepped Metal Surfaces.* Physical Review Letters, 2010. **104**(18).
39. Lu, X., et al., *Layer-by-layer thinning of MoS_2 by thermal annealing.* Nanoscale, 2013. **5**(19): p. 8904-8908.

요 약 문

원자수준의 두께를 갖는 이황화 텅스텐 결정의 성장과정과 성질분석에 대한 연구

본 연구는 널리 알려진 이차원 물질 중 하나인 이황화 텅스텐 (WS_2) 단층의 성장과정과 성질을 분석한 내용을 담고 있다. 최근 몇 년간 금속의 성질을 띠는 그래핀의 약점을 대체할 수 있는 물질로 WS_2 같은 이차원 반도체가 제안되었고, 많은 연구가 진행되어왔다. WS_2 같은 이차원 반도체들은 원자 수준으로 얇고 투명하면서 직접천이를 하기 때문에 다양한 광전자 소자로 응용이 가능하다. 특히 WS_2는 다른 이차원 반도체들에 비해 뛰어난 광학적 성질이 보고되고 있어 잠재성이 높은 물질이다. 하지만 대면적의 단층 WS_2를 합성을 위해 핵 생성 및 성장 과정에 대한 이해는 아직 부족한 실정이다. 이 논문은 다양한 조건으로 WS_2를 성장 시키고 성질을 분석하여 핵 생성 및 성장에 대한 과정을 제안한다. 여러 조건의 시편으로부터 우리는 WS2 단층 성장과 핵 생성에 대해 3 가지의 사실을 알 수 있었다. 1) WS_2 2차원 성장은 삼각형 모양의 WS_2 박막 중심에 있는 핵에 의해서 쉽게 일어나고 이 핵은 단결정의 WS_2이다. 2) 단층의 WS_2성장에는 임계크기(20 μm)가 있는데 그 이유는 이차원 성장을 할 때 WS_2 분자가 표면을 확산하는 거리에 제한이 있는 것으로 보인다. 3) 광학적 분석을 통하여 품질이 높은 WS_2 합성 조건을 찾았다. 이 연구는 TMDCs 단층 성장 과정에 대한 새로운 방향을 제시하여 고품질의 대면적 단층 성장에 기여할 수 있을 것으로 기대된다.

Keywords: 이황화 텅스텐, 이차원 물질, 성장과정, 화학적 기상